RESEARCH ARTICLE

QUANTUM SIMULATION

Probing entanglement in a many-body–localized system

Alexander Lukin, Matthew Rispoli, Robert Schittko, M. Eric Tai, Adam M. Kaufman*, Soonwon Choi†, Vedika Khemani, Julian Léonard, Markus Greiner‡

An interacting quantum system that is subject to disorder may cease to thermalize owing to localization of its constituents, thereby marking the breakdown of thermodynamics. The key to understanding this phenomenon lies in the system's entanglement, which is experimentally challenging to measure. We realize such a many-body–localized system in a disordered Bose-Hubbard chain and characterize its entanglement properties through particle fluctuations and correlations. We observe that the particles become localized, suppressing transport and preventing the thermalization of subsystems. Notably, we measure the development of nonlocal correlations, whose evolution is consistent with a logarithmic growth of entanglement entropy, the hallmark of many-body localization. Our work experimentally establishes many-body localization as a qualitatively distinct phenomenon from localization in noninteracting, disordered systems.

Isolated quantum many-body systems maintain their initial global purity while undergoing unitary time evolution. However, the presence of interactions drives local thermalization: The coupling between any subsystem and its complement mimics the contact with a bath. This causes the subsystem's degrees of freedom to be ultimately described by a thermal ensemble, even if the full system is in a pure state (*1*–*3*). A consequence of thermalization is that local information about the initial state of the subsystem gets scrambled and transferred into nonlocal correlations that are only accessible through global observables (*4*–*6*).

Disordered systems (*7*–*18*) can provide an exception to this paradigm of quantum thermalization. In such systems, particles can localize and transport ceases, which prevents thermalization. This phenomenon is called many-body localization (MBL) (*6*, *7*, *19*–*23*). Experimental studies have identified MBL through the persistence of the initial density distribution (*24*–*29*) and two-point correlation functions during transient dynamics (*25*). However, while particle transport is frozen, the presence of interactions gives rise to slow coherent many-body dynamics that generate nonlocal correlations, which are inaccessible to local observables (*30*–*32*). These dynamics are considered to be the hallmark of MBL and distinguish it from its noninteracting counterpart, called Anderson localization (*7*–*11*, *14*, *15*, *18*). Their observation, however, has remained elusive because it requires exquisite control over the system's coherence.

We study these many-body dynamics by probing the entanglement properties of an MBL system with a fixed particle number (*30*–*34*). We distinguish two types of entanglement that can exist between a subsystem and its complement (Fig. 1A): (i) Number entanglement implies that the particle number in one subsystem is correlated with the particle number in the other. This type of entanglement is generated through tunneling across the boundary between the subsystems. (ii) Configurational entanglement implies that the configuration of the particles in one subsystem is correlated with the configuration of the particles in the other. It therefore requires the presence of at least one particle in each subsystem. Tunneling alone does not generate configurational entanglement, as it acts individually on each particle. Interactions, in contrast, can entangle pairs of particles. As a result, the combination of tunneling and interactions can lead to configurational entanglement at long distances.

The formation of particle and configurational entanglement changes in the presence or absence of interactions and disorder in the system (Fig. 1B). In thermal systems without disorder, interacting particles delocalize and rapidly create both types of entanglement throughout the entire system. In contrast, for Anderson localization, number entanglement builds up only locally at the boundary between the two subsystems. Here, the lack of interactions prevents the formation of a substantial amount of configurational entanglement. In MBL systems, number entanglement builds up in a similarly local way as for Anderson localization. However, notably, the presence of interactions additionally enables the slow formation of configurational entanglement throughout the entire system.

In this work, we realize an MBL system and characterize its key properties: breakdown of quantum thermalization, finite localization length of the particles, area-law scaling of the number entanglement, and slow growth of the configurational entanglement that ultimately results in a volume-law scaling. The first three properties are also present for an Anderson localized state; the slowly growing configurational entanglement

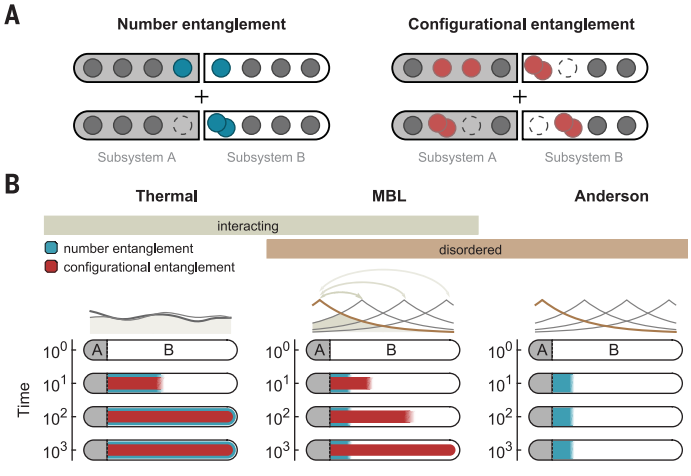

Fig. 1. Entanglement dynamics in nonequilibrium quantum systems. (**A**) Subsystems A and B of an isolated system out of equilibrium entangle in two different ways: Number entanglement stems from a superposition of states with different particle numbers in the subsystems and is generated through particle motion across the boundary; configurational entanglement stems from a superposition of states with different particle arrangement in the subsystems and requires both particle motion and interactions. (**B**) In the absence of disorder, both types of entanglement rapidly spread across the entire system owing to delocalization of particles (left). The degree of entanglement and the time scales change drastically when applying disorder (center): Particle localization spatially restricts number entanglement, yet interactions allow configurational entanglement to form very slowly across the entire system. A disordered system without interactions shows only local number entanglement, whereas the slow growth of configurational entanglement is completely absent (right).

Department of Physics, Harvard University, Cambridge, MA 02138, USA.
*Present address: JILA, National Institute of Standards and Technology and University of Colorado, and Department of Physics, University of Colorado, Boulder, CO 80309, USA.
†Present address: Department of Physics, University of California, Berkeley, CA 94720, USA.
‡Corresponding author. Email: greiner@physics.harvard.edu

qualitatively distinguishes our system from a noninteracting, localized state.

Experimental system

In our experiments, we study MBL in the interacting Aubry-André model for bosons in one dimension (*35*, *36*), which is described by the Hamiltonian

$$\hat{\mathcal{H}} = -J\sum_i(\hat{a}_i^\dagger\hat{a}_{i+1} + h.c.) + \frac{U}{2}\sum_i \hat{n}_i(\hat{n}_i - 1) + W\sum_i h_i\hat{n}_i \quad (1)$$

where $\hat{a}_i^\dagger$ ($\hat{a}_i$) is the creation (annihilation) operator for a boson on site i, and $\hat{n}_i = \hat{a}_i^\dagger\hat{a}_i$ is the particle number operator on that site. The first term describes the tunneling between neighboring lattice sites with the rate $J/\hbar$, where $\hbar$ is the reduced Planck constant. The second term represents the energy shift U when multiple particles occupy the same site. The last term introduces a site-resolved potential offset, which is created with an incommensurate lattice $h_i = \cos(2\pi\beta i + \phi)$ of period $1/\beta \approx 1.618$ lattice sites, phase ϕ, and amplitude W. In our system, we achieve independent control over J, W, and ϕ (Fig. 2A).

Our experiments begin with a Mott-insulating state in the atomic limit with one ^{87}Rb atom on each site of a two-dimensional optical lattice (Fig. 2B). The system is placed in the focus of a high-resolution imaging system through which we project site-resolved optical potentials (*37*). We first isolate a single, one-dimensional chain from the Mott insulator and then add the site-resolved potential offsets W_i with the incommensurate lattice. At this point, the system remains in a product state of one atom per lattice site. We abruptly switch on the tunneling by reducing the lattice depth within a fraction of the tunneling time (Fig. 2C). This quench brings the system to a nonequilibrium state and initializes the unitary time dynamics corresponding to the above Hamiltonian. The tunneling time $\tau = \hbar/J = 4.3(1)$ ms and the interaction strength $U = 2.87(3)J$ remain constant in all our experiments. After a variable evolution time, we abruptly increase the lattice depth and image the system in an atom number–sensitive way with single-site resolution (*38*). This projects the many-body state onto the number basis, which consists of all possible distributions of the particles within the chain.

In some realizations, particle loss during the time evolution and imperfect readout reduce the number of detected atoms compared with the initial state, thereby injecting classical entropy into the system. We eliminate this entropy by postselecting the data on the intended atom number, thereby reaching a fidelity of 99.1(2)% unity filling in the initial state, which is limited by the fraction of doublon-hole pairs in the Mott insulator. The result is a highly pure state, in which all correlations are expected to stem from entanglement in the system.

Breakdown of thermalization

We first investigate the breakdown of thermalization in a subsystem that consists of a single lattice site. The conserved total atom number enforces a one-to-one correspondence between the particle number outcome on a single site and the number in the remainder of the system, entangling the two during tunneling dynamics. Ignoring information about the remaining system puts the subsystem into a mixed state of different number states. The associated number entropy is given by $S_n^{(1)} = -\sum_n p_n \log(p_n)$, where p_n is the probability of finding n atoms in the subsystem (*38*). Because the atom number is the only degree of freedom of a single lattice site, $S_n^{(1)}$ captures all of the entanglement between the subsystem and its complement and is equivalent to the single-site von Neumann entanglement entropy $S_{vN}^{(1)}$.

Counting the atom number on an individual lattice site in different experimental realizations allows us to obtain the probabilities p_n and compute $S_{vN}^{(1)}$. We perform such measurements for various evolution times. At low disorder depth $[W = 1.0(1)J]$, the entropy grows over a few tunneling times and then reaches a stationary

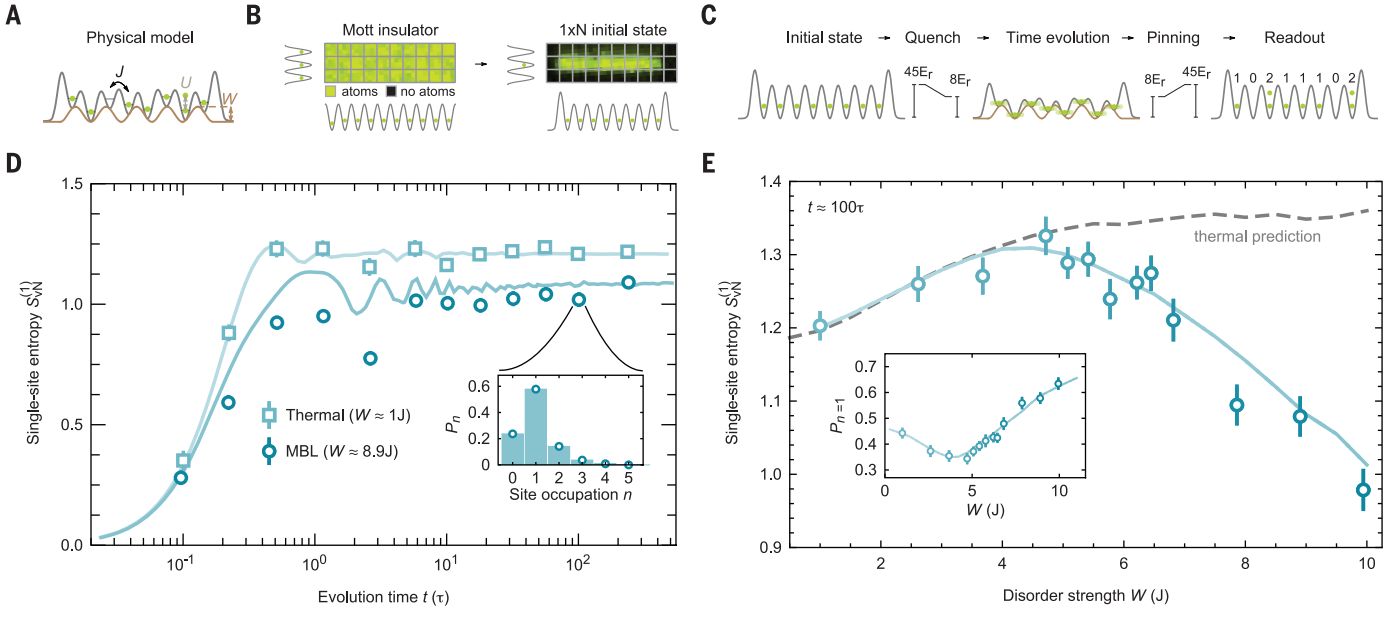

Fig. 2. Site-resolved measurement of thermalization breakdown. (**A**) One-dimensional Aubry-André model with particle tunneling rate $J/\hbar$, on-site interaction energy U, and quasi-periodic potential with amplitude W. (**B**) We prepare the initial state of eight unentangled atoms by projecting tailored optical potentials onto a two-dimensional Mott insulator at $45E_r$ lattice depth, where $E_r = h \times 1.24$ kHz is the recoil energy. (**C**) We create a nonequilibrium system by abruptly enabling tunneling dynamics. After a variable evolution time, we project the many-body state back onto the number basis by increasing the lattice depth and obtain the site-resolved atom number from a fluorescence image (*38*). (**D**) Single-site von Neumann entropy $S_{vN}^{(1)}$ computed from the site-resolved atom number statistics (inset) after different evolution times (scaled with tunneling time $\tau = \hbar/J$) in the presence of weak and strong disorder. (**E**) Inset: Probability p_1 of retrieving the initial state; main panel: $S_{vN}^{(1)}$ as a function of W and measured after 100τ. The deviation from the thermal-ensemble prediction for strong disorder signals the breakdown of thermalization in the system. All lines in (C) and (D) show the prediction of exact diagonalization calculations without any free parameters. Each data point is sampled from 197 disorder realizations (*38*). Error bars denote the SEM.

value (Fig. 2D). The stationary value is reduced for strong disorder [$W = 8.9(1)J$] and remains constant in time over two decades of time evolution up to several hundred tunneling times. The lack of entropy increase indicates the absence of heating in the system. The excellent agreement of the measured entropy with ab initio calculations up to the longest measured evolution times suggests a highly unitary evolution of the system.

We perform measurements of $S_{vN}^{(1)}$ at different disorder strengths after an evolution of 100 tunneling times (Fig. 2E). To evaluate the degree of local thermalization, we compare the results with the prediction of a thermal ensemble for our system (*38*). For weak disorder, the measured entropy agrees with the predicted value, whereas the entropy is significantly reduced from the thermal value for strong disorder, signaling the absence of thermalization in the system. A reduced entropy implies that the subsystem does not occupy all available degrees of freedom and retains some memory of its initial conditions for arbitrarily long evolution times. We indeed find that the probability of retrieving the initial state of one atom per site increases for strong disorder (Fig. 2E, inset).

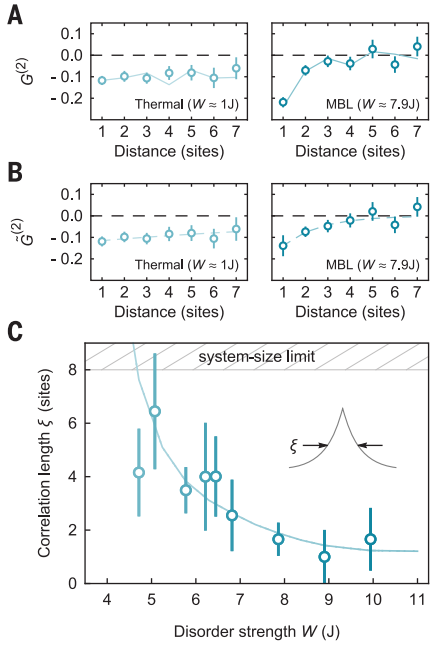

Fig. 3. Spatial localization of the particles. (**A**) The density-density correlations $G^{(2)}(d)$ for the eight-site system as a function of distance d at weak (left) and strong (right) disorder after an evolution time of 100τ. The alternating nature of the density-density correlations is imprinted by the autocorrelation function of the quasi-periodic potential. (**B**) We retrieve a clean exponential decay of the correlation function by subtracting the contribution of the quasi-periodic potential (see main text). The dashed line shows the result of an exponential fit. (**C**) Correlation length ξ, extracted by fitting the raw data [see (A)] and similar data for other disorder strengths with a function that takes the effect of the quasi-periodic potential into account (see main text). Each measurement is sampled from 197 disorder realizations (*38*). The solid lines in (A) and (C) show the prediction of exact diagonalization, calculated without any free parameters (*38*), whereas the dashed lines in (B) show the result of the exponential fit to the data (see main text). Error bars denote the SEM in (A) and (B) and the fit error in (C).

Spatial localization

The breakdown of thermalization is expected to be a consequence of the spatial localization of the particles. Previous experiments have determined the decay length of an initially prepared density step into empty space (*27*). We measure the localization by directly probing density-density correlations within the system. These correlations are captured by $G^{(2)}(d) = \langle n_i n_{i+d}\rangle - \langle n_i\rangle\langle n_{i+d}\rangle$, where $\langle\ldots\rangle$ denotes averaging over different disorder realizations as well as all sites i of the chain. The particle numbers on two sites at distance $d > 0$ are uncorrelated for $G^{(2)}(d) = 0$. If a particle moves a distance d, the sites become anticorrelated, and the correlator decreases to $G^{(2)}(d) < 0$.

We measure the density-density correlations $G^{(2)}(d)$ for different disorder strengths in the stationary regime (Fig. 3A). For low disorder, we find the correlations to be independent of distance and below zero. This indicates that the particles tunnel across the entire system and hence are delocalized. By contrast, at strong disorder, only nearby sites show significant correlations, signaling the absence of particle motion across large distances. We thus conclude that the particles are localized. The decay of the density correlations with distance shows a nonmonotonous behavior that is determined by the quasi-periodic potential. We take this effect into account by fitting the data with an exponentially decaying function $G_{fit}^{(2)} = (c_1 + c_2 V_2(d)) \times e^{-d/\xi}$, with free parameters c_1, c_2, and ξ, such that the amplitude at distance d is scaled by the autocorrelation function $V_2(d)$ of the quasi-periodic potential (*38*). We eliminate the contribution coming from the disorder potential by defining $\tilde{G}^{(2)}(d) = G^{(2)}(d) - c_2 V_2(d) e^{-d/\xi}$, which indeed shows an exponential decay in the localized regime (Fig. 3B) (*38*). We show the fitted localization length as a function of the disorder strength (Fig. 3C). For increasing disorder, the correlation length decreases from the entire system size down to around one lattice site.

Our observation of localized particles is consistent with the description of MBL in terms of local integrals of motion (*30*–*32*). It describes the global eigenstates as product states of exponentially localized orbitals. The correlation length extracted from our data is a measure of the size of these orbitals. Because the localized orbitals form a complete set of locally conserved quantities, this picture connects the breakdown of thermalization in MBL with nonthermalizing, integrable systems.

Dynamics and spreading of entanglement

We now turn to a characterization of the entanglement properties of larger subsystems, starting with a subsystem covering half the system size. As for the case of a single lattice site, the particle number in the subsystem can become entangled with the number in the remaining system through tunneling dynamics, resulting in the number entropy $S_n = -\sum_n p_n \log(p_n)$. However, subsystems that extend over several lattice sites, with a given particle number, offer the particle configuration as an additional degree of freedom for the entanglement. Configurational entanglement only builds up substantially in interacting systems because configurational correlations require several particles. The associated configurational entropy S_c, together with the number entropy, forms the von Neumann entropy, $S_{vN} = S_n + S_c$ (*38*). An analogous relation exists for spin systems with conserved total magnetization instead of the particle number.

The dynamics of S_n and S_c in the MBL regime (Fig. 4A) can be understood in the picture of localized orbitals. Because the localized orbitals restrict the particle motion, the number entropy can only develop within the localization length; hence, S_n saturates at a lower value than for the thermal case. In addition, saturation is reached at a later time, since the disorder suppresses the tunneling. The dynamics of S_c are distinctively different. The bare on-site interaction and particle tunneling combine into an effective interaction among localized orbitals, which decays exponentially with the distance between them. As a consequence, entanglement between distant orbitals forms slowly, causing a logarithmic growth of S_c, even after S_n has saturated (*30*–*34*).

In our experiment, we can independently probe both types of entanglement. We obtain the number entropy S_n through the probabilities p_n by counting the atom number in the subsystem in different experimental realizations. The configurational entropy S_c, in contrast, is challenging to measure in a many-body system because it requires experimental access to the coherences between a large number of quantum states (*39*, *40*). Here, we choose a complementary approach to probe the configurational entanglement in the system. It exploits the configurational correlations between the subsystems, quantified by the correlator (*38*)

$$C = \sum_{n=0}^{N} p_n \sum_{\{A_n\}\{B_n\}} |p(A_n \otimes B_n) - p(A_n)p(B_n)| \quad (2)$$

where $\{A_n\}$ ($\{B_n\}$) is the set of all possible configurations of n particles in subsystem A ($N - n$ in B), and N is the total number of particles in the system. All probability distributions are normalized within the subspaces of n particles in A and the remaining $N - n$ particles in B. The configuration $A_n \otimes B_n$ is separable if $p(A_n \otimes B_n) = p(A_n)p(B_n)$. The correlator therefore probes the

entanglement through the deviation from separability between A and B. In the MBL regime, for sufficiently small amounts of entanglement, we numerically find C to be proportional to S_c; hence, it inherits its scaling properties (*38*). Our measurements lie within the numerically verified parameter regime. Even for large systems, one can find a regime of proportionality between C and S_c by reducing the interaction strength, the evolution time, or the subsystem size or by increasing the disorder strength. This implies that configurational correlations present a powerful tool to study entanglement in many-body–localized systems based on density correlations.

We study the time dynamics of S_n and C with and without disorder (Fig. 4, B and C). Without disorder, both S_n and C rapidly rise and reach a stationary value within a few tunneling times (insets). In the presence of strong disorder, we find a qualitatively different behavior for the two quantities: S_n reaches a stationary state within a few tunneling times, although after a longer evolution time than in the thermal case owing to reduced effective tunneling. Additionally, the stationary value is significantly reduced, indicating suppressed particle transport through the system. The correlator C, in contrast, shows a persistent slow growth up to the longest evolution times reached by our measurements. The growth is consistent with logarithmic behavior over two decades of time evolution. We conclude that we observe interaction-induced dynamics in the MBL regime that are consistent with the phenomenological model (*30*–*32*). The agreement of the long-term dynamics of S_n and C with the numerical calculations in the MBL regime confirms the unitary evolution of the system over 100τ. The system remains in the finite-time limit, not in the finite-size limit, because the spread of entanglement has not yet stopped at the longest studied evolution times.

Considering the entropy in subsystems of different sizes gives us insights into the spatial distribution of entanglement in the system: In a one-dimensional system, locally generated entanglement results in a subsystem-size-independent entropy, whereas entanglement from nonlocal correlations causes the entropy to increase in proportion to the size of the subsystem. In reference to the subsystem's boundary and volume, these scalings are called area law and volume law. We find almost no change in S_n for different subsystems of an MBL system (Fig. 5A), indicating an area-law scaling confirming that particle transport is suppressed. In contrast, the configurational correlations C increase until the subsystem reaches half the system size (Fig. 5B). Such a volume-law scaling is also expected for the entanglement entropy and demonstrates that the observed logarithmic growth indeed stems from nonlocal correlations across the entire system.

Conclusion

Our method, which is based on measurements of the particle number fluctuations and their configurations, can be generalized to higher dimensions and different experimental platforms, where a direct measurement of entanglement entropy remains challenging (e.g., trapped ions, neutral atoms, and superconducting circuits). In the future, experiments at larger system sizes will be of interest to shed light on the critical

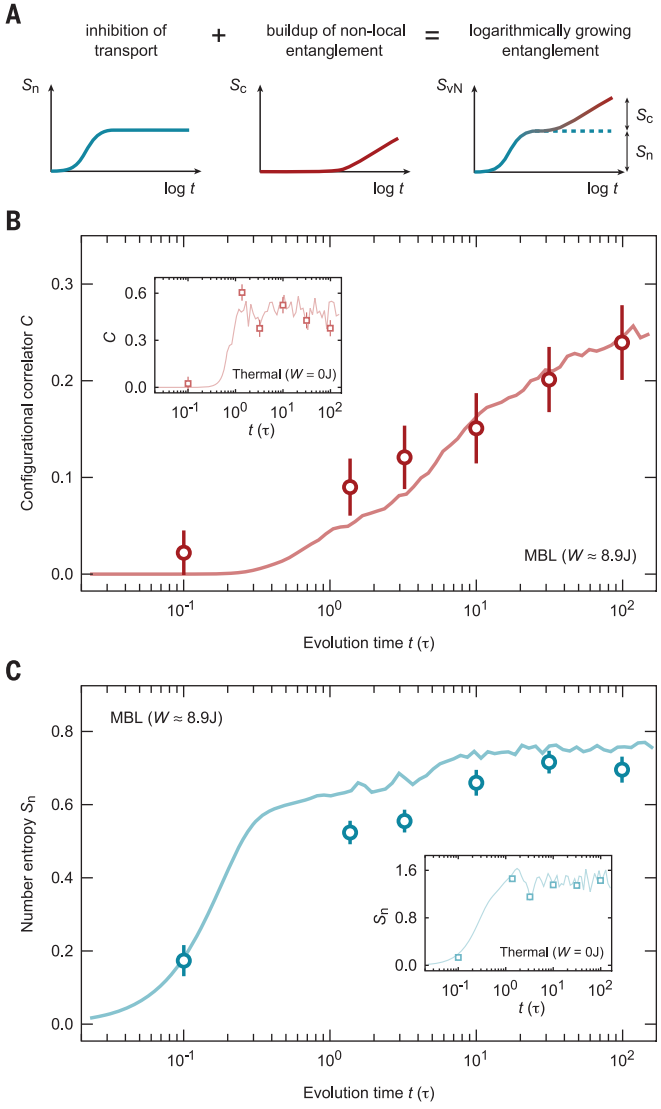

Fig. 4. Dynamics of number and configurational entanglement. (**A**) The von Neumann entanglement entropy is the sum of the number entropy and the configurational entropy, whose dynamics in an MBL system occur over different time scales (*38*). (**B**) We probe the configurational entropy with the correlator C. At strong disorder, it shows a persistent slow increase that is consistent with a logarithmic growth in time until the longest evolution times covered by our measurements. (**C**) The number entropy S_n reaches a stationary value within a few tunneling times. Without disorder, the entanglement dynamics change: Both S_n and C quickly reach a stationary value (insets). The solid lines show the prediction of exact diagonalization calculations without any free parameters (*38*). The above data were taken on a six-site system and averaged over four disorder realizations. Error bars denote the SEM.

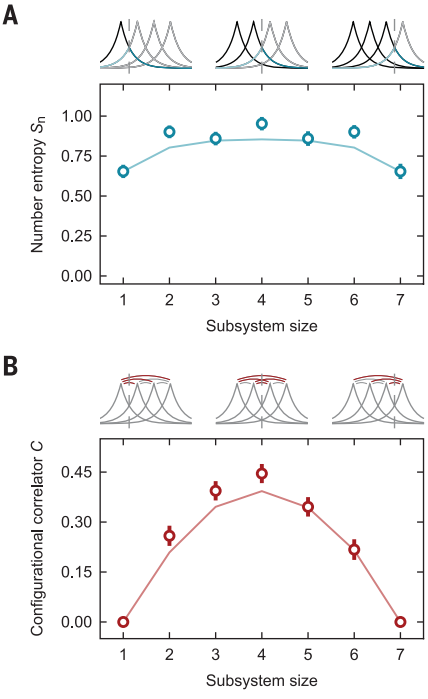

Fig. 5. Spatial distribution of the entanglement. Number entropy and configurational correlator in the eight-site MBL system ($W = 8.9\ J$) after an evolution time of 100τ. (**A**) The number entropy S_n barely depends on the subsystem size (i.e., follows an area law). (**B**) The configurational correlator C increases almost linearly with the subsystem size, showing a volume-law behavior. The solid lines show the prediction of exact diagonalization calculations without any free parameters (*38*). The above data were averaged over four disorder realizations. Error bars denote the SEM and are below the marker size if hidden.

properties of the thermal-to-MBL phase transition, which are the subject of ongoing studies (*41*–*44*). In our system, it is experimentally feasible to increase the system size at unity filling to a numerically intractable regime. Additionally, the full control over the disorder potential on every site opens the way to studying the role of rare regions and Griffiths dynamics as well as the long-time behavior of an MBL state with a link to a thermal bath (*45*–*47*). Ultimately, these studies will further our understanding of quantum thermodynamics and whether such systems are suitable for future applications as quantum memories (*6*).

REFERENCES AND NOTES

1. J. M. Deutsch, *Phys. Rev. A* **43**, 2046–2049 (1991).
2. M. Srednicki, *Phys. Rev. E Stat. Phys. Plasmas Fluids Relat. Interdiscip. Topics* **50**, 888–901 (1994).
3. M. Rigol, V. Dunjko, M. Olshanii, *Nature* **452**, 854–858 (2008).
4. C. Neill *et al*., *Nat. Phys.* **12**, 1037–1041 (2016).
5. A. M. Kaufman *et al*., *Science* **353**, 794–800 (2016).
6. R. Nandkishore, D. A. Huse, *Annu. Rev. Condens. Matter Phys.* **6**, 15–38 (2015).
7. P. W. Anderson, *Phys. Rev.* **109**, 1492–1505 (1958).
8. T. Schwartz, G. Bartal, S. Fishman, M. Segev, *Nature* **446**, 52–55 (2007).
9. J. Billy *et al*., *Nature* **453**, 891–894 (2008).
10. G. Roati *et al*., *Nature* **453**, 895–898 (2008).
11. Y. Lahini *et al*., *Phys. Rev. Lett.* **100**, 013906 (2008).
12. B. Deissler *et al*., *Nat. Phys.* **6**, 354–358 (2010).
13. B. Gadway, D. Pertot, J. Reeves, M. Vogt, D. Schneble, *Phys. Rev. Lett.* **107**, 145306 (2011).
14. S. S. Kondov, W. R. McGehee, J. J. Zirbel, B. DeMarco, *Science* **334**, 66–68 (2011).
15. F. Jendrzejewski *et al*., *Nat. Phys.* **8**, 398–403 (2012).
16. C. D'Errico *et al*., *Phys. Rev. Lett.* **113**, 095301 (2014).
17. S. S. Kondov, W. R. McGehee, W. Xu, B. DeMarco, *Phys. Rev. Lett.* **114**, 083002 (2015).
18. G. Semeghini *et al*., *Nat. Phys.* **11**, 554–559 (2015).
19. I. V. Gornyi, A. D. Mirlin, D. G. Polyakov, *Phys. Rev. Lett.* **95**, 206603 (2005).
20. D. M. Basko, I. L. Aleiner, B. L. Altshuler, *Ann. Phys.* **321**, 1126–1205 (2006).
21. V. Oganesyan, D. A. Huse, *Phys. Rev. B* **75**, 115111 (2007).
22. E. Altman, R. Vosk, *Annu. Rev. Condens. Matter Phys.* **6**, 383–409 (2015).
23. D. A. Abanin, E. Altman, I. Bloch, M. Serbyn, arXiv:1804.11065 [cond-mat.dis-nn] (30 April 2018).
24. M. Schreiber *et al*., *Science* **349**, 842–845 (2015).
25. J. Smith *et al*., *Nat. Phys.* **12**, 907–911 (2016).
26. P. Bordia *et al*., *Phys. Rev. Lett.* **116**, 140401 (2016).
27. J. Y. Choi *et al*., *Science* **352**, 1547–1552 (2016).
28. H. P. Lüschen *et al*., *Phys. Rev. X* **7**, 011034 (2017).
29. P. Bordia, H. Lüschen, U. Schneider, M. Knap, I. Bloch, *Nat. Phys.* **13**, 460–464 (2017).
30. M. Serbyn, Z. Papić, D. A. Abanin, *Phys. Rev. Lett.* **110**, 260601 (2013).
31. M. Serbyn, Z. Papić, D. A. Abanin, *Phys. Rev. Lett.* **111**, 127201 (2013).
32. D. A. Huse, R. Nandkishore, V. Oganesyan, *Phys. Rev. B* **90**, 174202 (2014).
33. M. Žnidarič, T. Prosen, P. Prelovšek, *Phys. Rev. B* **77**, 064426 (2008).
34. J. H. Bardarson, F. Pollmann, J. E. Moore, *Phys. Rev. Lett.* **109**, 017202 (2012).
35. S. Aubry, G. André, *Ann. Isr. Phys. Soc.* **3**, 133 (1980).
36. S. Iyer, V. Oganesyan, G. Refael, D. A. Huse, *Phys. Rev. B* **87**, 134202 (2013).
37. W. S. Bakr, J. I. Gillen, A. Peng, S. Fölling, M. Greiner, *Nature* **462**, 74–77 (2009).
38. Materials and methods are available as supplementary materials.
39. R. Islam *et al*., *Nature* **528**, 77–83 (2015).
40. A. Elben, B. Vermersch, M. Dalmonte, J. I. Cirac, P. Zoller, *Phys. Rev. Lett.* **120**, 050406 (2018).
41. R. Vosk, D. A. Huse, E. Altman, *Phys. Rev. X* **5**, 031032 (2015).
42. A. C. Potter, R. Vasseur, S. A. Parameswaran, *Phys. Rev. X* **5**, 031033 (2015).
43. V. Khemani, S. P. Lim, D. N. Sheng, D. A. Huse, *Phys. Rev. X* **7**, 021013 (2017).
44. H. P. Lüschen *et al*., *Phys. Rev. Lett.* **119**, 260401 (2017).
45. K. Agarwal *et al*., *Ann. Phys.* **529**, 1600326 (2017).
46. W. De Roeck, F. Huveneers, *Phys. Rev. B* **95**, 155129 (2017).
47. R. Nandkishore, S. Gopalakrishnan, *Ann. Phys. (Berlin)* **529**, 1600181 (2017).
48. A. Lukin *et al*., Probing entanglement in a many-body-localized system, Zenodo (2019); https://doi.org/10.5281/zenodo.2565132

ACKNOWLEDGMENTS

We acknowledge discussions with I. Cirac, E. Demler, J. Eisert, C. Gross, W. W. Ho, H. Pichler, D. A. Huse, and A. Polkovnikov. **Funding:** We are supported by grants from the National Science Foundation, the Gordon and Betty Moore Foundations EPiQS Initiative, an Air Force Office of Scientific Research MURI program, an Army Research Office MURI program, and the NSF Graduate Research Fellowship Program. J.L. acknowledges support from the Swiss National Science Foundation. V.K. acknowledges support from the Harvard Society of Fellows and the William F. Milton Fund. **Author contributions:** A.L., M.R., R.S., M.E.T., and J.L. performed the experiment and collected and analyzed data. All authors contributed to discussion of the data, development of the theoretical concepts, and writing of the manuscript. M.G. supervised the project. **Competing interests:** The authors declare no competing interests. **Data and materials availability:** Published data are available on the Zenodo public database (*48*).

SUPPLEMENTARY MATERIALS

science.sciencemag.org/content/364/6437/256/suppl/DC1
Materials and Methods
Supplementary Text
Figs. S1 to S12
Table S1
References (*49*–*55*)

4 May 2018; accepted 20 March 2019
10.1126/science.aau0818

Probing entanglement in a many-body–localized system

Alexander Lukin, Matthew Rispoli, Robert Schittko, M. Eric Tai, Adam M. Kaufman, Soonwon Choi, Vedika Khemani, Julian Léonard and Markus Greiner

Science **364** (6437), 256-260.
DOI: 10.1126/science.aau0818

A logarithmic signature

Some one-dimensional disordered interacting quantum systems have been theoretically predicted to display a property termed many-body localization (MBL), where the system retains the memory of its initial state and fails to thermalize. However, proving experimentally that something does not occur is tricky. Instead, physicists have proposed monitoring the entanglement entropy of the system, which should grow logarithmically with evolution time in an MBL system. Lukin *et al.* observed this characteristic logarithmic trend in a disordered chain of interacting atoms of rubidium-87. This method should be generalizable to other experimental platforms and higher dimensions.

Science, this issue p. 256